Document downloaded from:

http://hdl.handle.net/10251/122256

This paper must be cited as:

Capilla Romá, MT.; Talavera Usano, CF.; Ginestar Peiro, D.; Verdú Martín, GJ. (2018). Numerical analysis of the 2D C5G7 MOX benchmark using PL equations and a nodal collocation method. Annals of Nuclear Energy. 114:32-41. https://doi.org/10.1016/j.anucene.2017.12.002

The final publication is available at

https://doi.org/10.1016/j.anucene.2017.12.002

Copyright Elsevier

Additional Information

Numerical analysis of the 2D C5G7 MOX benchmark using P_L equations and a nodal collocation method

M. T. Capilla[a], C. F. Talavera[a], D. Ginestar[a], G. Verdú[b,*]

[a]*Departamento de Matemática Aplicada, Universitat Politècnica de València, Camino de Vera 14, E-46022 Valencia, Spain*
[b]*Departamento de Ingeniería Química y Nuclear, Universitat Politècnica de València, Camino de Vera 14, E-46022 Valencia, Spain*

Abstract

A classical discretization for the angular dependence of the neutron transport equation is based on a truncated spherical harmonics expansion. The resulting system of equations are the P_L equations. We review the multi-dimensional P_L equations, for arbitrary odd order L, and then we proceed to the spatial discretization of these equations, for rectangular geometries, using a nodal collocation method based on the expansion of the spatial dependence of the fields in terms of orthonormal Legendre polynomials. The validity of the method to deal with complex reactor problems is then studied with the seven-group 2D NEA C5G7 MOX fuel assembly benchmark problem. The solution is computed for different spatial meshes, showing that the P_L results are consistent with the reference Monte Carlo solution. Additionally, the first subcritical modes are also computed for the the full reactor configuration.

Keywords: Multi-dimensional P_L equations, Spherical harmonics method, Nodal collocation method, Criticality calculations, C5G7 MOX benchmark

1. Introduction

The physics involved in the neutron interactions of a nuclear reactor core are modelled by the Boltzmann neutron transport equation, which is a integro-differential neutron balance equation in a space of three spatial

*Corresponding author. Tel.: 34-963877630; fax: 34-963877639.
Email addresses: tcapilla@mat.upv.es (M. T. Capilla), talavera@mat.upv.es (C. F. Talavera), dginesta@mat.upv.es (D. Ginestar), gverdu@iqn.upv.es (G. Verdú)

variables, three angular variables and one energy variable. The computational solution of transport problems is difficult and complex and, except for academic problems, the solution of the transport equation is obtained using Monte Carlo methods (Spanier and Gelbard, 2008), deterministic methods such as discrete ordinate (S_N) methods, spherical harmonics (P_L) methods, or other numerical methods (Lewis and Miller, 1984). The two-group diffusion approximation is a classical and well established method of performing reactor calculations for the neutron multi-group transport problem, but this approximation is inaccurate in optically thin regions and where the gradient of the flux is large, so can produce large errors for heterogeneous cores with complex fuel assemblies or for another analysis as fine mesh (pin-by-pin) geometry.

The discrete ordinates method (S_N) when applied to transport problems has been used in numerous codes such as DANTSYS (Alcouffe et al., 1995), PENTRAN (Sjoden and Haghighat, 1996), DORT/TORT (Rhoades and Childs, 1993) and DENOVO (Evans et al., 2010). The main shortcoming of S_N codes are ray-effects (Lewis and Miller, 1984) that arise from the discrete angular directions of the method and give unphysical numerical artifacts in the computed scalar fluxes. The Monte Carlo methods are computationally expensive and do not provide complete flux solutions to the whole problem geometry (Briesmeister, 2000), but on the other hand can accurately compute integral quantities like k_{eff}, dose rate, etc. Recently, the methods of characteristics (DeHart, 2009) have been studied and implemented; the disadvantage of the method is the computational cost.

The P_L approximation to the transport equation is well known (Davison, 1957; Weinberger and Wigner, 1958; Clark and Hansen, 1964), and is based on the discretization of the angular dependence of the transport equation by a spherical harmonic expansion truncated to a finite order L. The linear system of equations that results from this expansion is known as the P_L equations. One advantage of the P_L equations is that they are, like the transport equation, rotationally invariant, and do not suffer from angular defects in the solution (ray effects). Moreover, the P_L equations formally converge (in L^2 norm) to the solution of the transport equation as $L \rightarrow \infty$ (Davison, 1960). In three-dimensional geometries (3D), P_L equations form a complex set of first-order equations, that can be rewritten as second-order differential equations, but the coupling involves not only the angular moments but also mixed spatial derivatives.

These complexities led to propose the simplified P_L (SP_L) approximation

(Gelbard, 1968), that eliminates cross-derivative terms in the equations and then simplifies the spatial discretization, usually giving accurate enough results, providing then a practical way to solve simplified transport problems; in fact, SP_L equations are "high-order asymptotic solutions of the transport equations" (Brantley and Larsen, 2000); the SP_L approximation actually implies that, "to the lowest order of approximation, the angular flux is invariant by rotations around the local axis" (Sánchez, 2009, p. 25). Unfortunately, SP_L equations are unable to deal with general 3D transport problems. It can be shown (Tomasević and Larsen, 1996) that the accuracy of the solution can not be increased with larger order L, and it is possible to obtain worse results with the SP_L approximation than with the diffusion equation.

The full P_L approximation provide the best solution, but at a cost of a complex computer implementation. Fletcher (1983) obtained a solution of the P_L equations removing odd-order fields and using the finite difference or finite element method to discretize the resulting equations. Ziver et al. (2005) implemented and solved in the code EVENT the spherical harmonics (P_L) equations using finite elements methods. Recently, in the work of Yousefi et al. (2017), the solution of the multi-dimensional even parity neutron transport equation is investigated. The even parity angular flux density is expanded in spherical harmonics polynomials, being the spatial variable approximated by finite element methods and the angular matrices by analytic integration. Furthermore, the 2D C5G7 benchmark problem is used for validation.

In this work, we first review the multi-dimensional spherical harmonics (P_L) equations. We must remember that the P_L equations can be developed in several manners. We have opted for a diffusive form of the P_L equations and we briefly describe the application of a nodal collocation method for these equations, based on the expansion of the spatial dependence of the fields in terms of orthonormal Legendre polynomials, for arbitrary odd order L. Only rectangular geometries will be discussed. The choice of odd integer order L guarantees continuity of the scalar neutron flux along material discontinuities of the reactor volume. For explicit calculations, the reader can consult previous works by the authors (Capilla et al., 2005, 2008, 2012), where the nodal collation method was developed.

One advantage of the method is that this approach reduces the dimension of the corresponding algebraic problem in comparison with other methods, like finite elements of finite differences, because of the lower dimension of the matrices. The method gives accurate results when discretization nodes of

big size are considered, using a moderate number of Legendre polynomials. Some drawbacks to the P_L equations are also commented, like oscillatory behavior of the solutions (Brunner, 2002).

The method is applied to criticality problems, where a generalized algebraic eigenvalue problem approximates the initial differential eigenvalue problem. Then, the k-effective and the stationary neutron flux distribution of the system can be numerically computed, and also the subcritical eigenvalues and their associated subcritical modes.

The method has been implemented into a computer code called SHNC (Spherical Harmonics-Nodal Collocation), that solves multi-dimensional multigroup eigenvalue problems and source problems. Furthermore, and for its application to the 2D C5G7 MOX benchmark problem, a new version of the SHNC code, based on P_L equations, has been parallelized using the SLEPc library (Hernández et al., 2005).

The rest of the paper is organized as follows. In Section 2, we review the spherical harmonics method that is applied to the transport equation eigenvalue problem, resulting into the first order multi-dimensional P_L equations. These equations are then rewritten as vector-valued second order differential equations. The boundary conditions (vacuum and reflective) are then approximated by the spherical harmonics method. A nodal collocation method is then applied to the spatial dependence of P_L equations. The method is based on a truncated Legendre polynomials expansion of the fields. The result of this discretization method is to replace the transport equation problem by a large and sparse linear algebraic problem. In order to show the capabilities of the methodology to treat realistic reactor problems, in Section 3 the performance of the method is validated with a detailed pin-cell geometry 2D C5G7 MOX reactor eigenvalue problem. Finally, in Section 4 we establish our conclusions.

2. The transport equation and the P_L equations

In this section we review the multi-dimensional P_L equations, for arbitrary angular order L, that will be formulated as a vector-valued second order differential equation.

2.1. The Boltzmann transport equation

The physical phenomena of neutron transport and interactions in the reactor core are modelled by the Boltzmann transport equation (Stacey, 2001),

which is an integro-differential neutron balance equation in a space of seven dimensions. For a typical criticality calculation, where the k-effective and the neutron distribution for a stationary configuration of a multiplying system are determined, Boltzmann equation becomes the following steady state eigenvalue problem (Stacey, 2001):

$$\vec{\Omega}\,\vec{\nabla}\Phi(\vec{r},\vec{\Omega},E)+\Sigma_t(\vec{r},E)\,\Phi(\vec{r},\vec{\Omega},E)=Q_s(\vec{r},\vec{\Omega},E)+\frac{1}{\lambda}Q_f(\vec{r},\vec{\Omega},E)\,,\ \vec{r}\in V\,. \tag{1}$$

$$\Phi(\vec{r},\vec{\Omega},E)=0\,,\quad \text{for all } \vec{\Omega}\,\vec{n}\leq 0,\ \vec{r}\in\partial V\,, \tag{2}$$

where V is the volume of the system and $\vec{n}$ is the outward pointing normal vector at the outside boundary of the system ∂V. Eq. (1) must be supplemented with appropriate boundary conditions; for example, Eq. (2) describes vacuum boundary conditions, where there is no incoming neutron angular flux. Here $\Phi(\vec{r},\vec{\Omega},E)$ is the neutron angular flux at location $\vec{r}=(x_1,x_2,x_3)$ (using Cartesian coordinates), in the direction of travel given by the unit vector $\vec{\Omega}=(\cos\varphi\,\sin\theta\,,\,\sin\varphi\,\sin\theta\,,\,\cos\theta)$, $0<\varphi<2\pi$, $0<\theta<\pi$; Σ_t is the total macroscopic cross-section; and Q_s and Q_f are the scattering source term and the source of neutrons by fission term respectively, given by

$$Q_s(\vec{r},\vec{\Omega},E)=\int dE'\int d\vec{\Omega}'\,\Sigma_s(\vec{r};\vec{\Omega}',E'\to\vec{\Omega},E)\,\Phi(\vec{r},\vec{\Omega}',E')\,,$$
$$Q_f(\vec{r},\vec{\Omega},E)=\frac{\chi_p(E)}{4\pi}\int dE'\,\nu\Sigma_f(\vec{r},E')\int d\vec{\Omega}'\,\Phi(\vec{r},\vec{\Omega}',E')\,,$$

where Σ_s is the scattering cross-section from $(\vec{\Omega}',E')$ to $(\vec{\Omega},E)$; Σ_f is the fission cross-section; ν is the average number of neutrons per fission and χ_p is the fission spectrum. The largest value of λ for which a nonnegative fundamental mode solution of problem (1-2) exists will be denoted as $k_{\text{eff}}=\lambda_{\max}$.

The numerical solution of Eq. (1) requires a discretization of the six independent variables. First of all, the energy E is discretized into a finite number of energy groups such that $E\in[E_g,E_{g-1}[$, $g=1,2,\ldots,G$, with $E_0=+\infty$, $E_G=0$. This is known as the energy multi-group approximation. For simplicity, in what follows we will consider one energy group, and we will drop the dependence of Φ on energy.

2.2. The spherical harmonics method

The discretization of the angular dependence of the neutronic flux $\Phi(\vec{r},\vec{\Omega})$ is treated in a rotationally invariant way by a spherical harmonics expansion

$$\Phi(\vec{r},\vec{\Omega}) = \sum_{l=0}^{\infty} \sum_{m=-l}^{+l} \phi_{lm}(\vec{r})\, Y_l^m(\vec{\Omega})\,, \tag{3}$$

where $Y_l^m(\vec{\Omega}) = H_l^m\, P_l^m(\cos\theta) e^{im\varphi}$ are the (complex) spherical harmonics, $P_l^m(\cos\theta)$ are the associated Legendre polynomials and $H_l^m = \sqrt{\frac{(2l+1)}{4\pi}\frac{(l-m)!}{(l+m)!}}$. If we assume that scattering depends only on the relative angle between the incident and the scattered neutrons, $\vec{\Omega}\,\vec{\Omega}'$, then

$$\Sigma_s(\vec{r},\vec{\Omega}\,\vec{\Omega}') = \sum_{l=0}^{\infty} \frac{2l+1}{4\pi} \Sigma_{s,l}(\vec{r})\, P_l(\vec{\Omega}\,\vec{\Omega}')\,,$$

where P_l are Legendre polynomials.

These expansions are then inserted into Eq. (1) and, using the orthogonality properties of the spherical harmonics, the following set of (complex) equations for ϕ_{lm} is obtained:

$$\begin{aligned}
&\frac{1}{2}\Big(-C_1(l+1,m+1)\frac{\partial\phi_{l+1,m+1}}{\partial x_1} + C_2(l,m)\frac{\partial\phi_{l-1,m+1}}{\partial x_1} \\
&\qquad - C_1(l,m)\frac{\partial\phi_{l-1,m-1}}{\partial x_1} + C_2(l+1,m-1)\frac{\partial\phi_{l+1,m-1}}{\partial x_1}\Big) \\
&+ \frac{1}{2i}\Big(-C_1(l+1,m+1)\frac{\partial\phi_{l+1,m+1}}{\partial x_2} + C_2(l,m)\frac{\partial\phi_{l-1,m+1}}{\partial x_2} \\
&\qquad - C_1(l,m)\frac{\partial\phi_{l-1,m-1}}{\partial x_2} + C_2(l+1,m-1)\frac{\partial\phi_{l+1,m-1}}{\partial x_2}\Big) \\
&+ C_3(l+1,m)\frac{\partial\phi_{l+1,m}}{\partial x_3} + C_3(l,m)\frac{\partial\phi_{l-1,m}}{\partial x_3} + \Sigma_t\,\phi_{lm} \\
&\quad = \Sigma_{s,l}\,\phi_{lm} + \frac{1}{\lambda}\delta_{l0}\delta_{m0}\,\nu\Sigma_f\,\phi_{00}\,, \qquad l = 0,1,\ldots\,, \quad m = -l,\ldots,+l\,,
\end{aligned} \tag{4}$$

where

$$C_1(l,m) = \left(\frac{(l+m)(l+m-1)}{(2l+1)(2l-1)}\right)^{1/2}\,, \quad C_2(l,m) = C_1(l,-m)\,,$$
$$C_3(l,m) = \left(\frac{(l+m)(l-m)}{(2l+1)(2l-1)}\right)^{1/2}\,.$$

(It is assumed in Eqs. (4) that $\phi_{lm} = 0$ for invalid indices, $l < 0$ or $|m| > l$). A numerical treatment of these equations requires a finite approximation, so the series are truncated at some finite order $l = L$, i.e., $\phi_{lm} = \Sigma_{s,l} = 0$ for $l > L$ (the so-called P_L closure condition (Reed, 1972)) and the resulting equations are known as the (complex) P_L equations. In the following, we will only consider L to be an odd integer because it guarantees (see interface conditions, Sec. 2.3) continuity of even order moments and, in particular, continuity of the neutronic flux $\int \Phi \, d\vec{\Omega} = \sqrt{4\pi}\, \phi_{00}$ along the reactor volume.

We will now obtain the real form of P_L equations (4). The neutron angular flux Φ must be a real function, then ${\phi_{lm}}^* = (-1)^m \phi_{l,-m}$ and there are only $2l + 1$ real independent moments ϕ_{lm} for each $l > 0$, that is, $\{\phi_{l0}, \mathrm{Re}\, \phi_{lm}, \mathrm{Im}\, \phi_{lm}, m = 1, \ldots, l\}$. If we define the real moments

$$\begin{aligned} \xi_{lm} &= \mathrm{Re}\, \phi_{lm} = \frac{1}{2}(\phi_{lm} + (-1)^m \phi_{l,-m}) \,, \quad l = 0, 1, \ldots, L \,, \\ \eta_{lm} &= \mathrm{Im}\, \phi_{lm} = \frac{1}{2i}(\phi_{lm} - (-1)^m \phi_{l,-m}) \,, \quad l = 1, \ldots, L \,, \end{aligned} \tag{5}$$

and real vectors of even/odd l moments

$$X = (\xi_{l,m\geq 0}, \eta_{l,m>0})_{l=\mathrm{even}} \quad \text{and} \quad \bar{X} = (\xi_{l,m\geq 0}, \eta_{l,m>0})_{l=\mathrm{odd}}$$

with $\dim(X) = n_e = \frac{L(L+1)}{2}$ and $\dim(\bar{X}) = n_o = \frac{(L+1)(L+2)}{2} = n_e + L + 1$ for odd L then, taking real and imaginary part in Eqs. (4), we obtain the real P_L equations that can be written as the following set of vector-valued first order differential equations:

$$\sum_{j=1}^{3} M_j \frac{\partial \bar{X}}{\partial x_j} + \Sigma_a \, X = \frac{1}{\lambda} \, \mathrm{diag}(\delta_{l0} \, \nu\Sigma_f)_{l=\mathrm{even}} \, X \,, \tag{6}$$

$$\sum_{j=1}^{3} \bar{M}_j \frac{\partial X}{\partial x_j} + \bar{\Sigma}_a \, \bar{X} = 0 \,, \tag{7}$$

where $\Sigma_a = \mathrm{diag}(\Sigma_t - \Sigma_{sl})_{l=\mathrm{even}}$, $\bar{\Sigma}_a = \mathrm{diag}(\Sigma_t - \Sigma_{sl})_{l=\mathrm{odd}}$ are square diagonal matrices, and M_j and $\bar{M}_j$ are numerical rectangular matrices (of dimension $n_e \times n_o$ and $n_o \times n_e$, respectively) defined from the coefficients of Eqs. (4). Eq. (7) is a generalization of Fick's law,

$$\bar{X} = -D \sum_{j=1}^{3} \bar{M}_j \frac{\partial X}{\partial x_j} \,, \tag{8}$$

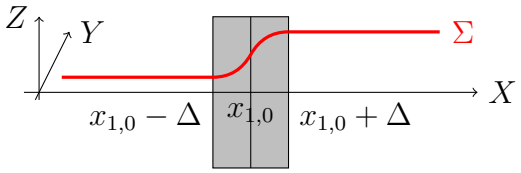

Figure 1: A transition region is inserted when a discontinuity occurs at $x_{1,0}$.

where $D = \bar{\Sigma}_a^{-1} = [\mathrm{diag}(\Sigma_t - \Sigma_{sl})_{l=\mathrm{odd}}]^{-1}$. If we replace Eq. (8) into Eq. (6) we obtain the diffusive form of P_L equations:

$$-\sum_{i,j=1}^{3} \frac{\partial}{\partial x_i}\Big(M_i D \bar{M}_j \frac{\partial X}{\partial x_j}\Big) + \Sigma_a\, X = \frac{1}{\lambda}\,\mathrm{diag}(\delta_{l0}\,\nu\Sigma_f)_{l=\mathrm{even}} X\,, \tag{9}$$

which is a second order vector-valued differential equation. Notice that the (square) effective diffusion matrices $M_i D \bar{M}_j$ are the analogous of the diffusion coefficient $[3(\Sigma_t - \Sigma_{s1})]^{-1}$ of P_1 equation for $L > 1$.

2.3. Interface conditions

At points where the internal source or any cross-section is discontinuous Eqs. (6) and (7) are undefined, and we will require some sort of interface conditions for these regions. Let us replace the interface with a very thin transition region, where the physical properties of the medium change rapidly, but continuously (Greenspan, 1968). If, for example, the discontinuity occurs at the YZ plane with coordinate $x_1 = x_{1,0}$, the transition region extends from $x_{1,0} - \Delta$ to $x_{1,0} + \Delta$, see Fig. 1. On integrating the P_L equations (6) and (7) over the transition region,

$$\int_{x_{1,0}-\Delta}^{x_{1,0}+\Delta} \Big[\sum_{j=1}^{3} M_j \frac{\partial \bar{X}}{\partial x_j} + \Sigma_a\, X\Big]\, dx_1 = \frac{1}{\lambda}\int_{x_{1,0}-\Delta}^{x_{1,0}+\Delta} \Big[\mathrm{diag}(\delta_{l0}\,\nu\Sigma_f)_{l=\mathrm{even}}\, X\Big]\, dx_1\,,$$

$$\int_{x_{1,0}-\Delta}^{x_{1,0}+\Delta} \Big[\sum_{j=1}^{3} \bar{M}_j \frac{\partial X}{\partial x_j} + \bar{\Sigma}_a\, \bar{X}\Big]\, dx_1 = 0\,,$$

we get

$$M_1\big(\bar{X}(x_{1,0}+\Delta)-\bar{X}(x_{1,0}-\Delta)\big)+\int_{x_{1,0}-\Delta}^{x_{1,0}+\Delta}\Big[\sum_{j=2}^{3}M_j\frac{\partial\bar{X}}{\partial x_j}+\Sigma_a\,X\Big]\,dx_1$$
$$=\frac{1}{\lambda}\int_{x_{1,0}-\Delta}^{x_{1,0}+\Delta}\Big[\mathrm{diag}(\delta_{l0}\,\nu\Sigma_f)_{l=\mathrm{even}}\,X\Big]\,dx_1\,,$$
$$\bar{M}_1\big(X(x_{1,0}+\Delta)-X(x_{1,0}-\Delta)\big)+\int_{x_{1,0}-\Delta}^{x_{1,0}+\Delta}\Big[\sum_{j=2}^{3}\bar{M}_j\frac{\partial X}{\partial x_j}+\bar{\Sigma}_a\,\bar{X}\Big]\,dx_1=0\,.$$

As Δ goes to zero all integrands remain continuous at the transition region, therefore we arrive at the following *interface conditions*

$$\lim_{\Delta\to 0+}M_1\,\bar{X}(x_{1,0}+\Delta)=\lim_{\Delta\to 0+}M_1\,\bar{X}(x_{1,0}-\Delta)\,,\tag{10}$$
$$\lim_{\Delta\to 0+}\bar{M}_1\,X(x_{1,0}+\Delta)=\lim_{\Delta\to 0+}\bar{M}_1\,X(x_{1,0}-\Delta)\,.\tag{11}$$

But matrix $\bar{M}_1$, of dimension $n_o\times n_e$ (with $n_o>n_e$ for odd L approximation) has rank n_e, so the second equation implies continuity of even order moments X at the interface,

$$\lim_{\Delta\to 0+}X(x_{1,0}+\Delta)=\lim_{\Delta\to 0+}X(x_{1,0}-\Delta)\,.\tag{12}$$

On the other hand, as $\dim(M_1)=n_e\times n_o$, the first equation gives n_e linear relations between the n_o ($>n_e$) odd moments $\bar{X}$, so it is not possible to impose continuity of *all* the moments.

2.4. Boundary conditions

Two kind of boundary conditions will be used in this work: vacuum and reflective. Vacuum boundary conditions correspond to zero incoming angular neutronic flux, $\Phi(\vec{r},\vec{\Omega})=0$, for all $\vec{\Omega}\,\vec{n}\le 0$, where $\vec{r}\in\partial V$ and $\vec{n}$ is the outwardly directed unitary normal vector to the external surface. This condition can not be satisfied in an exact way by a finite spherical harmonics series so some approximation is required. A well-known approximation is given by Marshak's conditions (Stacey, 2001):

$$\int_{\vec{\Omega}\,\vec{n}\le 0}d\vec{\Omega}\;Y_l^{m*}(\vec{\Omega})\,\Phi(\vec{r},\vec{\Omega})=0\;,\tag{13}$$

for $l = 1, 3, 5, \ldots, L$ (odd) and $m = 0, 1, \ldots, l$ (we remove negative m index conditions because the neutronic flux Φ is a real function). For regions with prismatic geometry and from the symmetry $Y_l^m(-\vec{\Omega}) = (-1)^l Y_l^m(\vec{\Omega})$ we obtain that, for $l + l'$ even,

$$\int_{\vec{\Omega}\,\vec{n}\leq 0} d\vec{\Omega}\; Y_l^{m*}(\vec{\Omega})\, Y_{l'}^{m'}(\vec{\Omega}) = \frac{1}{2}\int d\vec{\Omega}\; Y_l^{m*}(\vec{\Omega})\, Y_{l'}^{m'}(\vec{\Omega}) = \frac{1}{2}\delta_{ll'}\,\delta_{mm'}\,. \qquad (14)$$

Inserting the expansion given by the equation (3) for Φ truncated up to a finite odd order L, into Marshak's conditions (13) and using (14), it results into the conditions

$$\frac{1}{2}\phi_{lm} + \sum_{\substack{l' \text{ even} \\ -l'\leq m'\leq l'}}^{L-1} \left(\int_{\vec{\Omega}\,\vec{n}\leq 0} d\vec{\Omega}\; Y_l^{m*}(\vec{\Omega})\, Y_{l'}^{m'}(\vec{\Omega})\right) \phi_{l'm'} = 0\,, \qquad (15)$$

for $l = 1, 3, 5, \ldots, L$ and $m = 0, 1, \ldots, l$. Taking real and imaginary part in (15), Marshak's conditions can be written as

$$\bar{X} + N\,X = 0\;, \qquad (16)$$

where real vectors X and $\bar{X}$ were previously defined, and N is a real rectangular matrix (of dimension $n_o \times n_e$) with matrix elements

$$N_{(lm),(l'm')} = 2\int_{\vec{\Omega}\,\vec{n}\leq 0} d\vec{\Omega}\; Y_l^{m*}(\vec{\Omega})\, Y_{l'}^{m'}(\vec{\Omega})$$

((lm), l odd, are row indices; $(l'm')$, l' even, are column indices, with appropriate ordering). In order to compute the numerical values of matrix N, we must specify the geometry of the boundary surface. For example, if the unitary normal vector $\vec{n}$ to the boundary surface points to negative Z axis,

$$N_{(lm),(l'm')} = (N_3^-)_{(lm),(l'm')} = 4\pi\delta_{mm'} H_l^m H_{l'}^m \int_0^1 d\mu\, P_l^m(\mu) P_{l'}^m(\mu)\,,$$

($\mu = \cos\theta$) is a real-valued matrix. In the particular case of P_1 approximation for planar geometry (the spatial variation of the neutronic angular flux is only in the Z direction) $l = 1$, $l' = 0$ (even) so $m' = m = 0$, $N_{(1m),(00)} = \delta_{m0}\frac{\sqrt{3}}{2}$, and Marshak's condition (16), using Fick's law (8), reduces to the usual form

$$-\frac{1}{\sqrt{3}(\Sigma_t - \Sigma_{s0})}\frac{\partial X}{\partial x_3} + \frac{\sqrt{3}}{2}X = 0\,, \quad \text{with } X = \xi_{0,0}.$$

If vector $\vec{n}$ points to positive Z axis, the corresponding matrix $N_3^+ = -N_3^-$ has opposite sign.

We treat the discontinuity between the external surface and the interior region by inserting a very thin transition region, as in Section 2.3. If, for example, the boundary surface has normal vector $\vec{n}$ pointing to Z axis and is located at $x_3 = x_{3,0}$, the transition region covers the interval $[x_{3,0}, x_{3,0} + \Delta]$. We obtain, reasoning as is Section 2.3, the following interface conditions:

$$\begin{aligned} \lim_{\Delta \to 0+} M_3 \, \bar{X}(x_{3,0} + \Delta) &= M_3 \, \bar{X}(x_{3,0}) \, , \\ \lim_{\Delta \to 0+} X(x_{3,0} + \Delta) &= X(x_{3,0}) \, , \end{aligned} \tag{17}$$

so X is continuous at the interface but, using Eq. (16), $\bar{X}$ satisfies the interface condition

$$\lim_{\Delta \to 0+} M_3 \, \bar{X}(x_{3,0} + \Delta) = -M_3 \, N_3^- \, X(x_{3,0}) \, , \tag{18}$$

that is, a system of n_e linear conditions.

Reflective boundary conditions applies when physical conditions are identical at both sides of a symmetry plane. Then $\Phi(\vec{r}, \vec{\Omega}) = \Phi(\vec{r}, \vec{\tilde{\Omega}})$, where $\vec{\tilde{\Omega}}$ is the reflected angular direction with respect to the symmetry plane. For example, if the normal vector $\vec{n}$ to the symmetry plane points to the negative Z axis, the symmetry condition is

$$\Phi(\vec{r}, \varphi, \theta) = \Phi(\vec{r}, \varphi, \pi - \theta) \ , \quad \text{for } 0 < \varphi < 2\pi \, , \ 0 < \theta < \pi/2 \, . \tag{19}$$

Inserting the spherical harmonics expansion for Φ, this equation is equivalent to the condition

$$\phi_{lm} = 0 \ , \qquad \text{whenever } l + m \text{ odd}, \tag{20}$$

for $l = 0, 1, \ldots$ and $m = 0, 1, \ldots, l$. The same condition is valid if vector $\vec{n}$ is pointing to the positive Z axis.

2.5. The nodal collocation method

The final step in the numerical approximation to Eq. (1) is the spatial discretization of P_L equations (9). The diffusive nature of this equation suggests that a nodal collocation method can be numerically efficient. This approach was previously used for the neutron diffusion equation (Hébert, 1987; Verdú et al., 1994) and generalized for eigenvalue problems associated

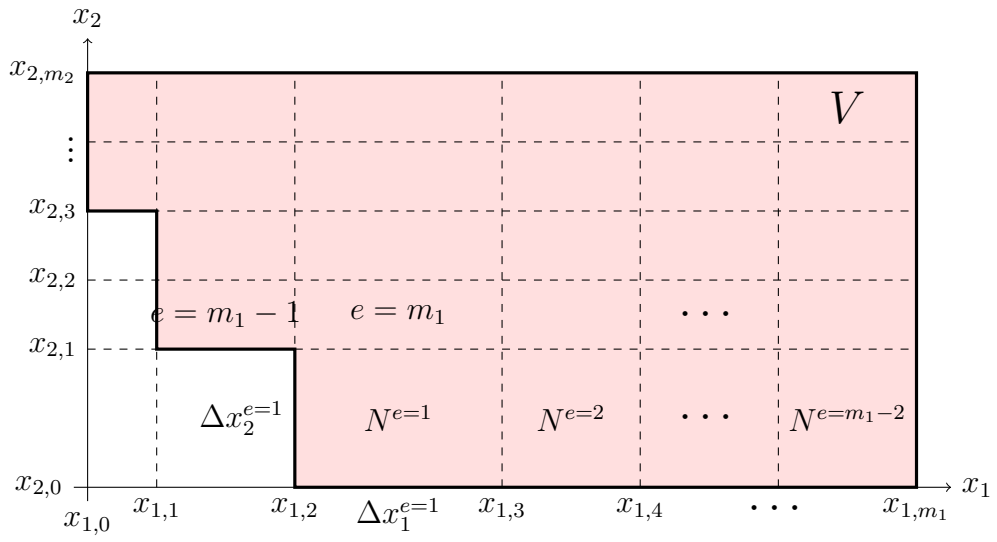

Figure 2: Sample rectilinear mesh covering the domain for 2D geometry. A *natural* ordering for spatial nodes N^e has been chosen.

to P_L equations in multi-dimensional rectangular geometries in (Capilla et al., 2005, 2008, 2012). We will give a short description of the key ideas of the method. For a detailed development, we refer to the references above mentioned.

We consider a domain that can be divided into N adjacent rectangular prisms, or nodes, of the form $N^e = [x_{1,i_1}, x_{1,i_1+1}]\times[x_{2,i_2}, x_{2,i_2+1}]\times[x_{3,i_3}, x_{3,i_3+1}]$, being $e = 1, \ldots, N$ the node index and $\{x_{1,i_1}, x_{2,i_2}, x_{3,i_3}\}$ the vertex coordinates of a rectilinear mesh ($i_j = 0, 1, \ldots, m_j$, for $j = 1, 2, 3$, are the vertex indices), see Fig. 2 for 2D geometry. The nodal collocation method assumes that on each node N^e the cross-sections in Eq. (1) are constant.

A generic node N^e is then transformed into the cubic node of volume one $N_u^e = [-\frac{1}{2}, +\frac{1}{2}]^3$ using the change of variables

$$u_j = \frac{1}{\Delta x_j^e}\Big(x_j - \frac{1}{2}(x_{j,i_j} + x_{j,i_j+1})\Big)\,, \quad j = 1, 2, 3\,, \tag{21}$$

where $\Delta x_j^e = x_{j,i_j+1} - x_{j,i_j}$,

For each node N_u^e, the change of variables (21) is then applied to the P_L equations (9). Furthermore, if $X^e(u_1, u_2, u_3)$ denotes the previously defined vector of l = even moments that appears in (9) for node N_u^e, its spatial

dependence is expanded in terms of (orthonormal) Legendre polynomials $\mathcal{P}_k(u) = \sqrt{2k+1}\,P_k(2u)$, $k = 0, 1, ...$ up to finite order M,

$$X^e(u_1, u_2, u_3) = \sum_{k_1,k_2,k_3=0}^{M} x^e_{k_1k_2k_3} \mathcal{P}_{k_1}(u_1)\,\mathcal{P}_{k_2}(u_2)\,\mathcal{P}_{k_3}(u_3)\,, \tag{22}$$

where $u_j \in [-\frac{1}{2}, +\frac{1}{2}]$, $j = 1, 2, 3$. The series (22) is then inserted into Eqs. (9) and equations for the unknowns to be determined, that is, the Legendre moments $x^e_{k_1k_2k_3}$, are derived.

In performing this process, integration of "diagonal terms" in Eqs. (9), that is, $\Sigma_a\,X^e$ and $\mathrm{diag}(\delta_{l0}\,\nu\Sigma_f)_{l=\mathrm{even}}X^e$, and integration of second derivative terms when $i \neq j$, is straightforward using the orthonormality properties of $\mathcal{P}_k(u)$. On the other hand, integration of second derivative terms for node N^e_u, when $i = j$, involves coupling with neighbouring nodes using interface conditions given by Eqs. (10) and (12). In the case that the node N^e_u is adjacent to an external boundary, then Marshak's conditions (16) and interface conditions (18) are used.

Finally, this procedure approximates Eqs. (9) by a generalized eigenvalue problem

$$\mathcal{A}\,V = \frac{1}{\lambda}\mathcal{B}\,V\ , \tag{23}$$

where V is a real vector of components $(\xi^{m;e}_{l;k_1k_2k_3}, \eta^{m;e}_{l;k_1k_2k_3})$ and $\mathcal{A}$, $\mathcal{B}$ are sparse real matrices of dimension $N \times G \times N_{\mathrm{Leg}} \times n_e$ (N is the number of nodes; G is the number of energy groups; $N_{\mathrm{Leg}} = M^d$ is the number of Legendre moments, with M the order in Legendre series (22) and d the spatial dimension and finally $n_e = L(L+1)/2 = \dim(X)$, being L the order of the P_L approximation).

3. Numerical results of the NEA 2D C5G7 benchmark

The numerical method exposed above has been implemented into the multi-group multi-dimensional FORTRAN 90 code SHNC (Spherical Harmonics-Nodal Collocation), that computes and solves the discretized generalized real non-symmetric eigenvalue problem (23), that is formulated as $\mathcal{B}\,V = \lambda\,\mathcal{A}\,V$, for an arbitrary P_L approximation, with odd L. The largest eigenvalue $\lambda \in \mathbb{R}$ is numerically computed on uniprocessor systems using ARPACK subroutines (Lehoucq et al., 1998). Linear systems are iteratively solved

using the bi-conjugate gradient stabilized method (BCGSTAB), with incomplete LU factorization (ILUT) as preconditioner, from the FORTRAN library SPARSKIT (Saad, 1994). Very large eigenvalue problems are effectively computed in parallel using the software library SLEPc (Hernández et al., 2005), that is based on the PETSc (Balay et al., 2016) data structures and employs the MPI standard. A Krylov-Schur method was chosen as eigensolver and linear systems were iteratively solved with the BCGSTAB method using HYPRE BoomerAMG as parallel preconditioner. Computational times vary from some hours to a few days on a Xeon CPU E5-2650 using 8 cores. It was observed that, with respect to computational time, the code scales (almost) lineally with the numbers of computer cores up to 6 cores. Beyond this, an increase of the number of computer cores does not reduce the computational time, but has the advantage of increasing the amount of global memory available to the computer code. The code also solves the isotropic fixed source problem for an arbitrary P_L approximation for odd order L (Capilla et al., 2016).

In previous works, we studied several multi-dimensional problems to verify the accuracy and test the convergence of the spherical harmonics-nodal collocation method. The reader can consult Capilla et al. (2005, 2008), where we analyzed one and two dimensional eigenvalue problems, in particular we treated problems with anisotropic scattering or strong spatial heterogeneity. In Capilla et al. (2012), we analyzed the capability of the nodal collocation method to deal with three-dimensional realistic reactor problems.

To test the capability of our method to treat advanced reactor problems, we present in this work results of the seven-group 2D NEA C5G7 fuel assembly benchmark, which is a detailed pin-cell geometry MOX reactor. We remark that also the subcritical modes can be obtained with our code.

3.1. Description of the benchmark and discretization model

We will analyze the application of the SHNC code to solve the two dimensional version of the C5G7 fuel assembly benchmark, proposed by the Nuclear Energy Agency (NEA) of the Organization for Economic Cooperation and Development (OECD) to test the ability of modern transport methods and codes to treat reactor heterogeneous core problems without spatial homogenization above the fuel pin level (Lewis et al., 2001).

This benchmark problem has been analyzed with various code packages (OECD/NEA, 2003), and a very precise solution was obtained using the

Monte Carlo method implemented in MCNP code, providing the k_{eff} eigenvalue solution, and also the core pin power predictions and the related errors.

The configuration of the 2D C5G7 MOX benchmark consists of a core with two MOX and two UO_2 square fuel assemblies, surrounded by a water reflector (moderator) region, as it is shown in Fig. 3 for a quarter of the core. The overall dimensions of the quarter configuration are 64.26 cm $\times$ 64.26 cm. Vacuum boundary conditions are applied to the right and to the bottom boundaries, and reflective boundary conditions to the top and to the left boundaries. Each fuel assembly consists of 17×17 square fuel pin cells, with side length 1.26 cm. The geometry and composition of a fuel pin cell is shown in Fig. 3. Every fuel pin consists of a single moderator region outside a circular region with radius 0.54 cm (fuel-clad mix) representing a fuel pin, a fission chamber or a guide tube. The MOX assemblies have three enrichments of 4.3%, 7.0% and 8.7% and the UO_2 assemblies have one enrichment. The same moderator composition is used in all the fuel pin cells and in the region surrounding the assemblies.

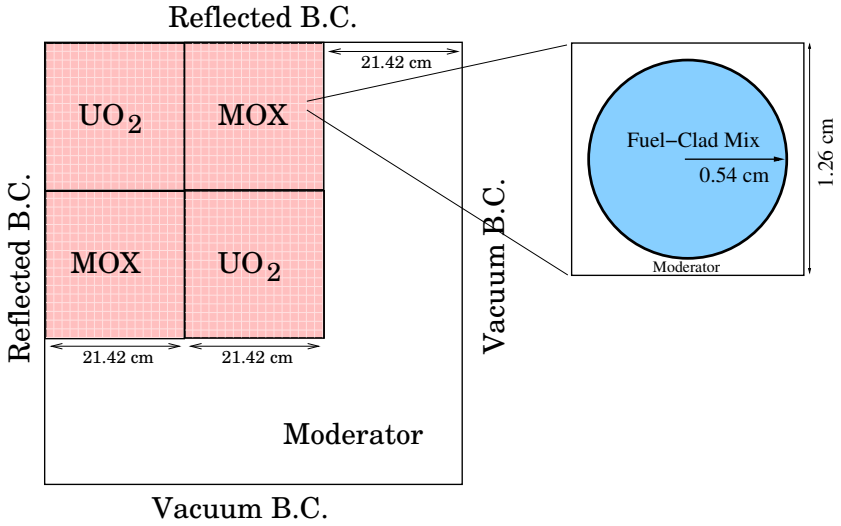

Figure 3: The core configuration for the 2D C5G7 benchmark problem and the fuel pin cell geometry.

More specifications about the seven-group, isotropic scattering cross-sections for UO_2, the three enrichments of MOX, the guide tubes, fission chamber and the moderator are provided in Lewis et al. (2001); OECD/NEA

(2003).

We present the solution of the 2D C5G7 benchmark problem, computed with the SHNC code, and the P_L results will be compared with the reference MCNP solutions (OECD/NEA, 2003) for k_{eff} eigenvalue, core pin power distribution and assembly average power. For the SHNC calculations, two different mesh discretizations of the pin cells were considered, both preserving the area of the circular region. Fig. 4(a) shows the rectangular mesh type A for a fuel pin cell, with 6×6 fine cartesian nodes (OECD/NEA, 2005). Fig. 4(b) shows the mesh type B, with the pin cell divided into 7×7 nodes resulting in a finer level of spatial resolution.

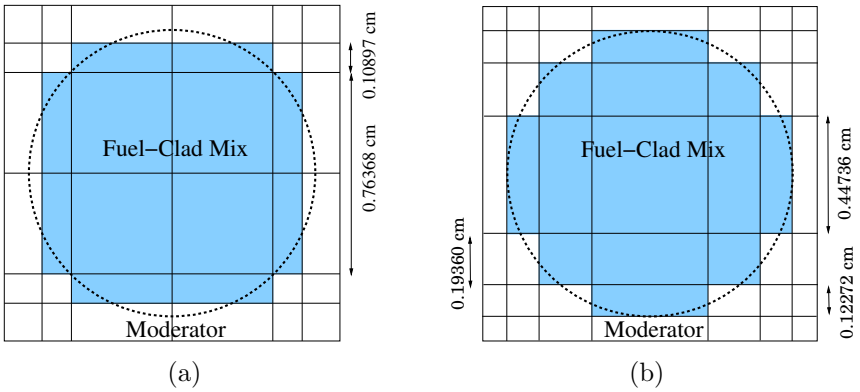

Figure 4: (a) Mesh A: SHNC spatial discretization by a 6×6 nodes, and (b) mesh B: spatial discretization by a 7×7 nodes.

To obtain reference cases with our method, the discretization according with meshes type A and B, were continued for every cell with a pin size in the moderator region, giving a calculation with $306 \times 306 = 93636$ nodes and $357 \times 357 = 127449$ nodes for the quarter reactor, named as meshes A1 and B1, respectively.

Starting from the discretizations A and B for the fuel pins, an alternative spatial discretization was considered throughout the moderator region, that is schematically described in Fig. 5 for mesh type B, and taken in a similar way for mesh type A. These models are named as A2 and B2. This problem has a highly anisotropic behaviour localized in the vicinities of MOX assemblies. Then, in order to obtain a smooth transition, in meshes A2 and B2, the fuel region nodalisation was continued for the first 6 neighbouring cells in the moderator, as can be seen in Fig. 5. The total number of nodes for the

quarter reactor is $251 \times 251 = 63001$ and $291 \times 291 = 84681$ for meshes A2 and B2, respectively. Then, for each type of the pin cell discretizations, A and B, we used two different models corresponding to different levels of spatial resolution for the moderator region extended to the right and below the outer assemblies. Meshes A2 and B2 give about a 34% reduction in the number of nodes with respect to meshes A1 and B1, and we will see that the calculations using meshes A2 and B2 maintain the same computational accuracy.

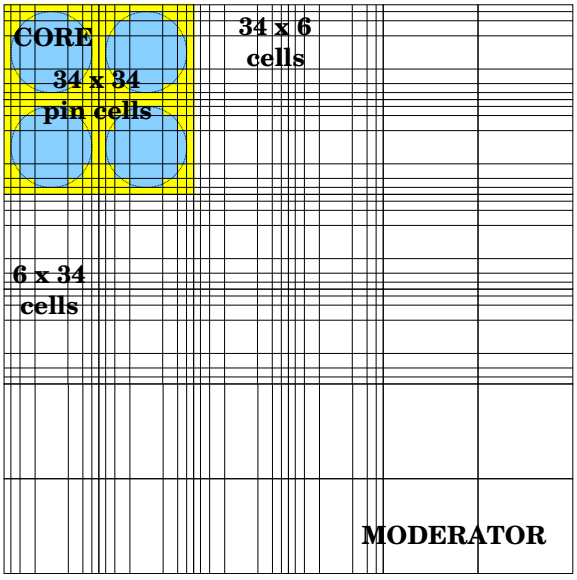

Figure 5: Scheme of the mesh B2, showing the grid of the moderator region, when the 7×7 pin cell nodalisation is taken.

3.2. 2D C5G7 results and analysis

Now we analyze the effect of the different spatial discretizations on the P_L solutions. Also, for each type of mesh, we study how changes in the Legendre polynomial order M in Eq. (22) affect the P_L results. Table 1 shows the k_{eff} eigenvalue results obtained with the P_1 and P_3 approximations, the reference MCNP solution and percent relative errors with respect to the reference solution, defined the last as $100(k_{\text{eff}}^{\text{SHNC}} - k_{\text{eff}}^{\text{Ref}})/k_{\text{eff}}^{\text{Ref}}$.

We observe that the results for k_{eff} with the P_3 approximation show smaller errors when the mesh type B is considered, then the increase of

Table 1: k_{eff} eigenvalue solutions and percent errors for the C5G7 benchmark problem computed with SHNC, for different spatial meshes and values of M

MCNP: $k_{\text{eff}} = 1.186550$ (± 0.008)					
SHNC	M	k_{eff} and percent error	SHNC	M	k_{eff} and percent error
		Mesh A1			Mesh A2
P_1	3	1.183922 (-0.221)	P_1	3	1.183700 (-0.240)
	4	1.183813 (-0.231)		4	1.183818 (-0.230)
P_3	3	1.180198 (-0.535)	P_3	3	1.180140 (-0.540)
	4	1.177268 (-0.782)		4	1.176693 (-0.830)
		Mesh B1			Mesh B2
P_1	3	1.183433 (-0.263)	P_1	3	1.183244 (-0.279)
	4	1.183056 (-0.294)		4	1.182943 (-0.304)
P_3	3	1.187656 ($+0.093$)	P_3	3	1.186949 ($+0.034$)
	4	1.183001 (-0.299)		4	1.181710 (-0.408)

the spatial resolution improves the P_3 results. However, no significant differences are observed between the P_1 results obtained with meshes type A and B. Then the spatial approximation of the pin cell has less impact on the quality of the calculations than the angular modelling. Better computational efficiency is obtained with meshes A2 and B2, that maintain almost the same accuracy as the calculations with meshes A1 and B1, while the computational time and memory required for the calculations is about a 34% lower. We can conclude that the P_L k_{eff} eigenvalue solutions in Table 1 for meshes B1 and B2 have an agreement with the MCNP solution using a 98% confidence interval. Although the results are consistent with the reference solution, our eigenvalue results show an oscillatory behaviour with the Legendre order M due to the polynomial origin of the spatial approximation.

Tables 2, 3 and 4 present results of the pin power, assembly power and percent errors, that help us to analyze the convergence and determine the precision of the P_L calculations. A direct comparison of the P_L pin power results against the reference solution in each individual pin, would be difficult because there are a total of 1056 fuel pins. Therefore, percent error measures were used in the form of average pin power percent error (AVG), root mean square (RMS) of the pin power percent error distribution and mean relative pin power percent error (MRE) (see OECD/NEA (2003)). Table 2 shows the pin power distribution error measures for the P_1 and P_3 solutions obtained

with the meshes A1 and B1, for different values of M, together with the reference MCNP solution. We observe that, as the angular order L increases, the error measures decrease approaching the MCNP reference values. Also, when the order M is increased from 3 to 4, the P_3 error measures improve with respect to the reference solutions.

Table 2: Pin power distribution error measures for the C5G7 benchmark

		AVG	RMS	MRE
MCNP		0.32	0.34	0.27
SHNC	M		Mesh A1	
P_1	3	1.47	1.78	1.27
	4	1.48	1.78	1.28
P_3	3	0.89	1.04	0.88
	4	0.63	0.74	0.61
SHNC	M		Mesh B1	
P_1	3	1.44	1.75	1.22
	4	1.43	1.77	1.18
P_3	3	1.14	1.34	1.15
	4	0.85	1.00	0.84

Table 3 tabulates the maximum pin power and the minimum pin power from the SHNC P_1 and P_3 solutions along with the reference MCNP solutions and percent relative errors. We also show in the table results from the ENTRANS code reported in Yousefi et al. (2017), where the even parity angular flux density is expanded in spherical harmonics polynomials, the angular matrices are treated by analytic integration and the spatial variable is treated using finite element method. The k_{eff} values obtained by (Yousefi et al., 2017, Table 6) were $k_{\text{eff}} = 1.18383$ (P_1) and $k_{\text{eff}} = 1.18416$ (P_3). We observe that an advantage of our method is that the maximum percent error in Table 3 is lower than in classical deterministic methods (OECD/NEA, 2003); this measure usually represents the largest deviations between Monte Carlo calculations.

Table 4 shows the P_L results for the assembly powers against the reference MCNP solutions.

In Table 5, we give the number of fuel pins that fall within the reference MCNP 68%, 95%, 99% and 99.9% confidence intervals. This information

Table 3: Specific pin powers and percent error results for the C5G7 benchmark problem

		Max. pin power	Percent error	Min. pin power	Percent error	Max. percent error
MCNP		2.498	±0.16	0.232	±0.58	
SHNC	P_1	2.525	1.09	0.240	3.77	5.92
	P_3	2.521	0.93	0.234	1.24	1.85
ENTRANS	P_1	2.520	0.881	0.242	4.310	NA
	P_3	2.533	1.401	0.236	1.724	NA

Table 4: Assembly power and percent error results for the C5G7 benchmark problem

		Inner UO_2	Percent error	MOX	Percent error	Outer UO_2	Percent error
MCNP		492.8	±0.10	211.7	±0.18	139.8	±0.20
SHNC	P_1	496.0	0.65	210.6	−0.52	138.8	−0.72
	P_3	495.5	0.54	210.5	−0.59	139.6	−0.10

shows the accuracy of the pin power distribution obtained with SHNC P_L approximation, giving the P_3 results greater number of fuel pins within the confidence intervals.

Table 5: Number of fuel pins within the reference confidence intervals for the C5G7 benchmark

SHNC	68%	95%	99%	99.9%
P_1	44	77	129	170
P_3	124	197	268	352

Fig. 6(a) shows the P_3 pin power distribution as a 3D graph. The power takes maximum values in the central core assembly. It is also observed that the power increases slightly in the area of the assemblies that is surrounded by moderator. In Fig. 6(b), we display the absolute values of the relative errors of P_3 pin power results with respect to the MCNP solution. We find that the largest relative errors are located in the proximities of the interface between the assemblies and the moderator region. The results of Fig. 6 and

those of Tables 3, 4 and 5 were obtained with the A1 reference mesh, and Legendre polynomial order $M = 4$.

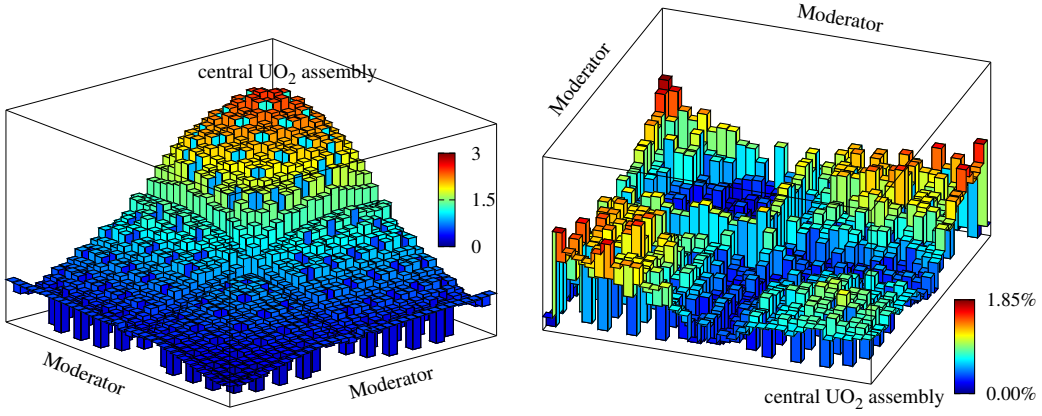

Figure 6: (a) P_3 pin power distribution for the C5G7 benchmark and (b) absolute value of the percent relative errors of the P_3 pin power values.

Figs. 7(a) and 7(b) show the contour plots of the P_3 scalar flux in fast (group 1) and thermal (group 7) energy groups, respectively. The obtained flux distribution was also calculated using mesh A1 and $M = 4$.

Due to the greater scattering cross-section in the moderator, the thermal scalar flux presents a peak in this region. The thermal flux in UO_2 assembly is higher than in MOX assembly, this is because the fast to thermal scattering cross-section in UO_2 is greater than in MOX. Fig.7(a) shows the maximum value of the flux distribution in the central UO_2 assembly, and it is reduced to the other assemblies and moderator region.

From the above results, we observe that the SHNC P_L approximation is able to reproduce the power distribution and the scalar flux reasonably well, obtaining consistent solutions for typical reactor calculations, where P_1 and P_3 are practical approximations. The remaining errors can be attributed to the high-order space-angle approximation necessary to solve this particular benchmark problem.

We have finally calculated the subcritical modes for the full reactor configuration. Table 6 shows the first dominant eigenvalues for this problem computed with P_1 and P_3 approximations using mesh A2 and $M = 4$. The presence of degenerate modes is due to the symmetry of the problem. Com-

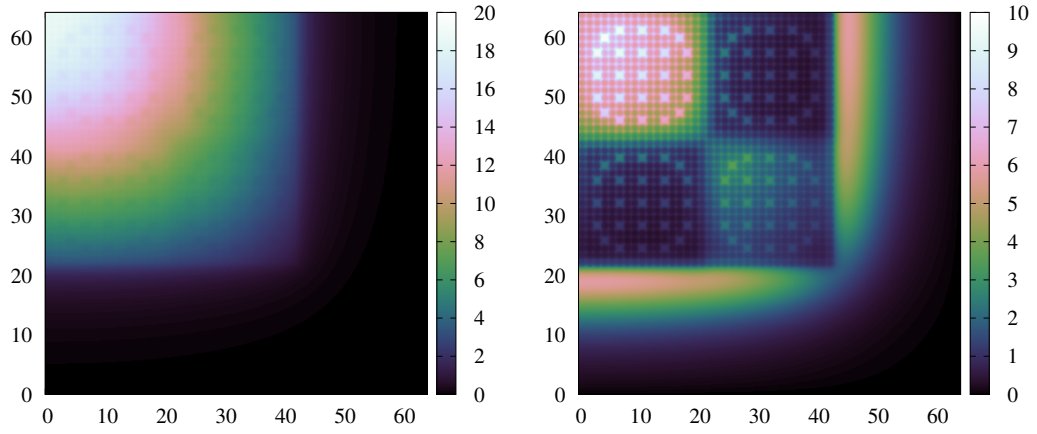

(a) Group 1 (b) Group 7

Figure 7: P_3 fast (a) and thermal (b) flux distribution for C5G7 benchmark problem.

puted relative errors $\frac{\|\mathcal{B}V-\lambda\mathcal{A}V\|}{\|\lambda V\|}$ for the subcritical modes reported by SLEPc code were $< 10^{-5}$ for P_1 approximation and $< 10^{-3}$ for P_3 approximation.

Table 6: First dominant eigenvalues for the 2D C5G7 benchmark problem

Eigenvalues	P_1	P_3
k_{eff}	1.183813	1.177268
2nd, 3rd	1.039234	1.039254
4th	0.949887	0.957624
5th	0.904549	0.915306
6th	0.859538	0.875609
7th, 8th	0.815803	0.827131

Figs. 8(a) and 8(b) display the contour maps of the eigenvectors corresponding to the second and fourth subcritical modes, respectively, using P_3 approximation, for energy groups 1 (fast) and 7 (thermal). We omit the third subcritical mode because, due to the symmetry of the reactor, it is obtained by rotating the second mode 90^o counterclockwise.

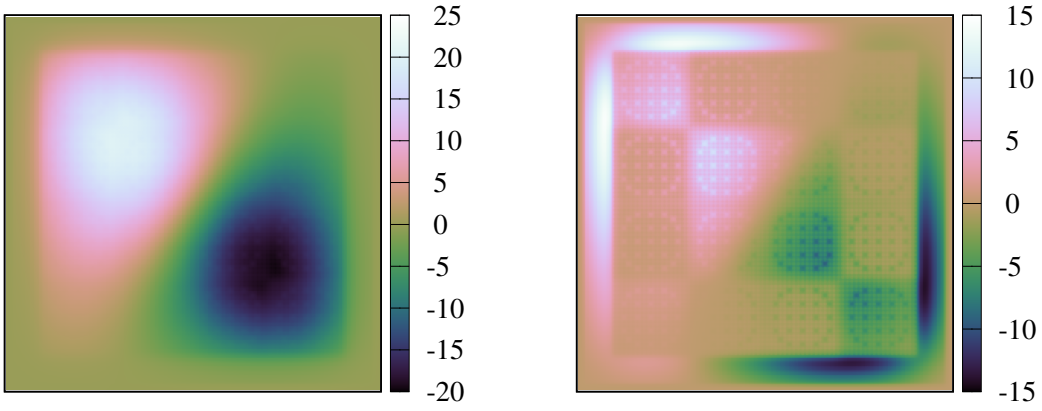

(a) Second eigenvector. Left: group 1; right: group 7.

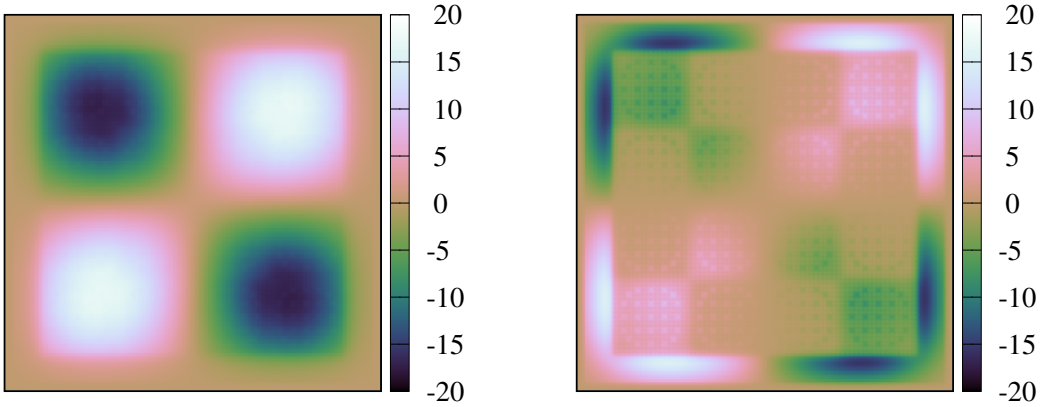

(b) Fourth eigenvector. Left: group 1; right: group 7.

Figure 8: P_3 eigenvectors for the 2nd and 4th subcritical modes for the C5G7 benchmark.

4. Conclusions

The application of a nodal collocation method for the diffusive form of the multi-dimensional spherical harmonics (P_L) equations has been reviewed. The method has been implemented into a computer code called SHNC, that solves multi-dimensional multi-group neutron eigenvalue problems and transport source problems in single-core and multiple-core computers.

The main advantages of the method are: P_L equations are invariant under rotations so there is no ray effect in the solutions. The method gives satisfactory results when nodes of big size are considered, using a moderate

number of Legendre polynomials. The lower dimension and good characteristics of the matrix associated to the algebraic problem, since this approach reduces the dimension of the corresponding algebraic problem in comparison to other methods, like finite elements or finite differences. This makes feasible to compute the first subcritical modes of the full reactor configuration, showing the degenerate modes that arise from the symmetry of the problem.

On the other hand, disadvantages of the method are: the relative complexity of the equations involved (that can be hidden with appropriate computer libraries), oscillatory behaviour of the solution of P_L equations, and unphysical negative values of the scalar flux, due to the polynomial nature of the spatial approximation. These issues will be addressed in future works.

In this work we have treated, for the first time with our method, the heterogeneous core reactor problem 2D C5G7 MOX fuel assembly benchmark, which is a realistic and computer intensive criticality benchmark problem. Although the results are consistent with the reference Monte Carlo solution, our P_L k_{eff} eigenvalue results show oscillatory behaviour with respect to the order L, due to the spectral nature of the P_L approximation. As was observed in other works, we notice that the spatial approximation of the pin cell has less impact on the quality of the calculations than the angular modelling. The SHNC P_1 and P_3 approximations reproduce the reference power distribution and the scalar flux reasonably well; the remaining errors are due to the high-order space-angle approximation necessary to solve this particular benchmark problem. An advantage of our method is that the pin power maximum percent error for this problem is lower than in classical deterministic methods.

In summary, the implementation of multi-dimensional P_L equations in the neutronic modules of reactor core simulators allows the analysis of complex heterogenous cores. The availability of fast computers will allow a more common use of this kind of methods to solve the neutron transport equation.

Acknowledgements

The authors express their gratitude to the anonymous reviewer for suggestions and helpful comments. This work has been partially supported by the Spanish Ministerio de Economía, Industria y Competitividad under project ENE2014-59442-P, and the Generalitat Valenciana under project PROMETEO11/2014/008.

References

Alcouffe, R.E., Baker, R.S., Brinkley, F.W., Marr, D.R., O'Dell, R.D., Walters, W.F., 1995. DANTSYS: A diffusion accelerated neutral particle transport code system. LA-12969-M, Los Alamos National Laboratory.

Balay, S., Abhyankar, S., Adams, M., Brown, J., Brune, P., Buschelman, K., Dalcin, L., Eijkhout, V., Gropp, W., Karpeyev, D., Kaushik, D., Knepley, M., McInnes, L.C., Rupp, K., Smith, B., Zampini, S., Zhang, H., Zhang, H., 2016. PETSc Users Manual. Technical Report ANL-95/11 - Revision 3.7, Argonne National Laboratory.

Brantley, P.S., Larsen, E.W., 2000. The simplified P_3 approximation. Nucl. Sci. Eng. 134, 1-21.

Briesmeister, J.F., 2000. MCNP–A general Monte Carlo N-particle Transport Code, version 4C. Technical Report LA-13709-M, Los Alamos National Laboratory.

Brunner, T.A., 2002. Forms of approximate radiation transport. Tech. Report SAND2002-1778, Sandia National Laboratories.

Capilla, M., Talavera, C.F., Ginestar, D., Verdú, G., 2005. A nodal collocation method for the calculation of the lambda modes of the P_L equations. Ann. Nucl. Energy 32, 1825–1853.

Capilla, M., Talavera, C.F., Ginestar, D., Verdú, G., 2008. A nodal collocation approximation for the multidimensional P_L equations – 2D applications. Ann. Nucl. Energy, 35:1820–1830.

Capilla, M., Talavera, C.F., Ginestar, D., Verdú, G., 2012. Application of a nodal collocation approximation for the multidimensional P_L equations to the 3D Takeda benchmark problems. Ann. Nucl. Energy 40, 1–13.

Capilla, M.T., Talavera, C.F., Ginestar, D., Verdú, G., 2016. Nodal collocation method for the multidimensional P_L equations applied to neutron transport source problems. Ann. Nucl. Energy 87, 89–100.

Clark, M.Jr., Hansen, K.F., 1964. Numerical Methods of Reactor Analysis. New York Academic, New York.

Davison, B., 1957. Neutron Transport Theory. Oxford University Press, London.

Davison, B., 1960. On the rate of convergence of the spherical harmonics method. Canad. J. Phys. 38, 1526–1545.

Evans, T.M., Stafford, A., Clarno, K.T., 2010. Denovo–A new three–dimensional parallel discrete ordinates code in SCALE. Nuclear Technology 171(2), 171–200.

DeHart, M.D., 2009. NEWT: A new transport algorithm for two–dimensional discrete ordinates analysis in non–orthogonal geometries. ORNL/TM–2005/39.

Fletcher, J.K., 1983. A solution of the neutron transport equation using spherical harmonics. J. Phys. A: Math. Gen. 16, 2827–2835.

Gelbard, E.M., 1968. Spherical harmonics methods: P_L and double P_L approximations. Computing Methods in Reactor Physics. Kelberg, D., Okrent, C. N. (eds.). Gordon and Breach, New York.

Greenspan, H., Kelber, C.N., Okrent, D., 1968. Computing Methods in Reactor Physics. Gordon & Breach Science Publishers, New York.

Hébert, A., 1987. Development of the nodal collocation method for solving the neutron diffusion equation. Ann. Nucl. Energy 14(10), 527–541.

Hernández, V., Román, J.E., Vidal, V., 2005. SLEPc: A scalable and flexible toolkit for the solution of eigenvalue problems. ACM Trans. Math. Soft. 31(3), 351–362.

Lehoucq, R.B., Sorensen, D.C., Yang, C., 1998. Arpack users' guide: Solution of large scale eigenvalue problems with implicitly restarted Arnoldi methods, SIAM, Philadelphia.

Lewis, E.E., Miller, W.F., 1984. Computational Methods of Neutron Transport. John Wiley and Sons, New York.

Lewis, E.E., Palmiotti, G., Taiwo, T.A., Smith, M.A., Tsoulfanidis, N., 2001. Specification for deterministic 2–D/3–D MOX fuel assembly transport calculations without spatial homogenization (C5G7 MOX). NEA/NSC/DOC (2001) 4.

OECD/NEA, 2003. Benchmark on deterministic transport calculations without spatial homogenisation. A 2–D/3–D MOX fuel assembly benchmark. NEA/NSC/DOC(2003) 16.

OECD/NEA, 2005. Benchmark on deterministic transport calculations without spatial homogenisation. MOX fuel assembly 3–D extension case. NEA/NSC/DOC(2005) 16.

Reed, Wm.H., 1972. Spherical harmonic solution of the neutron transport equation from discrete ordinate codes. Nucl. Sci. Energy 49, 10–19.

Rhoades, W.A., Childs, R.L., 1993. DORT/TORT two- and three-dimensional discrete ordinates transport, Version 2.7.3. ORNL, Oak Ridge, RSIC-CCC-543.

Saad, Y., 1994. SPARSKIT: a basic tool kit for sparse matrix computations–Version 2, http://www-users.cs.umn.edu/~saad/software/SPARSKIT.

Sánchez, R., 2009. Assembly homogenization techniques for core calculations. Prog. in Nucl. Energy 51, 14–31.

Sjoden, G.E., Haghighat, A., 1996. PENTRAN, A 3–D scalable transport code with complete phase space decomposition. Trans. Am. Nucl. Soc. 74.

Spanier, J., Gelbard, E.M., 2008. Monte Carlo principles and neutron transport problems. Dover Publications. Mineloa, NY.

Stacey, W.M., 2001. Nuclear Reactor Physics. Wiley, New York.

Tomasević, D.I., Larsen, E.W., 1996. The simplified P_2 approximation. Nucl. Sci. Eng. 122, 309–325.

Verdú, G., Ginestar, D., Vidal, V., Muñoz-Cobo, J.L., 1994. 3D λ modes of the neutron diffusion equation. Ann. Nucl. Energy 21(7), 405–421.

Weinberg, A.M., Wigner, E.P., 1958. The Physical Theory of Neutron Chain Reactors. Chicago University Press, Chicago.

Yousefi, M., Zolfaghari, A., Minuchehr, A., Abbasi, M.R., 2017. ENTRANS: A platform for finite elements modeling of 3D neutron transport equation, Part II. Multidimensional implementation. Ann. Nucl. Energy 101, 534–551.

Ziver, A.K., Shahdatullah, M.S., Eaton, M.D., Oliveira, C.R.E., Umpleby, C.C., Goddard, A.J.H., 2005. Finite element spherical harmonics (P_N) solutions of the three-dimensional Takeda benchmark problems. Ann. Nucl. Energy 32, 925–948.